NANO · MICRO small
www.small-journal.com

Electrically Conducting Elastomeric Fibers with High Stretchability and Stability

Sepideh Zokaei, Mariavittoria Craighero, Claudia Cea, Lucas M. Kneissl, Renee Kroon, Dion Khodagholy, Anja Lund, and Christian Müller**

Stretchable conducting materials are appealing for the design of unobtrusive wearable electronic devices. Conjugated polymers with oligoethylene glycol side chains are excellent candidate materials owing to their low elastic modulus and good compatibility with polar stretchable polymers. Here, electrically conducting elastomeric blend fibers with high stretchability, wet spun from a blend of a doped polar polythiophene with tetraethylene glycol side chains and a polyurethane are reported. The wet-spinning process is versatile, reproducible, scalable, and produces continuous filaments with a diameter ranging from 30 to 70 µm. The fibers are stretchable up to 480% even after chemical doping with iron(III) p-toluenesulfonate hexahydrate and exhibit an electrical conductivity of up to 7.4 S cm^{-1}, which represents a record combination of properties for conjugated polymer-based fibers. The fibers remain conductive during elongation until fiber fracture and display excellent long-term stability at ambient conditions. Cyclic stretching up to 50% strain for at least 400 strain cycles reveals that the doped fibers exhibit high cyclic stability and retain their electrical conductivity. Finally, a directional strain sensing device, which makes use of the linear increase in resistance of the fibers up to 120% strain is demonstrated.

1. Introduction

Stretchable electronic materials receive considerable interest for a wide range of areas from healthcare to wearable electronics,[1–7] including electronic skin and electronic textiles (e-skin and e-textiles).[8–13] To facilitate seamless bio-integration, materials are needed whose mechanical properties match the characteristics of skin or tissue. Specifically, such materials should i) be reversibly stretchable up to at least 50% to function, for example, on a knee joint,[4,14] ii) display a Young's modulus E in the same range as human skin and body tissue (for skin, E = 0.1–20 MPa),[15] and iii) be sufficiently robust to retain these characteristics during many cycles of tensile deformation. The polymer family of materials is uniquely suited in this context, as it offers a wide range of mechanical characteristics from E = 10 kPa and a strain at break ε_b = 4000% for elastomers, to E = 5 GPa and ε_b = 5% for engineering polymers.[16] The most stretchable conducting materials that have been realized are based on metal nanoparticle/elastomer composites[17–19] or poly(3,4-ethylenedioxythiophene):poly(styrenesulfonate) (PEDOT:PSS).[20–23]

The fiber format, which is needed for the realization of many e-textile devices, presents an additional challenge as the structural alignment introduced by the fiber spinning process typically results in a strong correlation between mechanical and electrical properties, that is, highly conducting fibers also have a high Young's modulus.[24] This correlation can be decoupled through the use of multi-component materials such as blends, nanocomposites, and coated substrates or templates, where one component provides the desired mechanical properties, for example, stretchability and elasticity, while the second component imparts electrical conductivity. It is essential that the conductivity is retained over a large strain range when the fiber is stretched. The change in conductivity leads to an additional important characteristic, the electrical stretchability ε_e, that is, the maximum strain at which the fiber remains conductive,[25] which in practice means that a finite conductance can be measured up to a certain strain.

Robust e-textiles will also need to be reversibly stretchable, both in terms of mechanical and electrical properties. The most common way to make stretchable conducting fibers is to combine an elastomer with a conducting material (e.g., a metal, carbon allotrope, or polymer), introduced by compounding,[26–28] blending,[7,29,30] coating,[31–33] or in situ polymerization.[34] An advantage offered by these methods is that they allow the use of conventional elastomers, with well-defined characteristics, as the matrix or substrate.[35] Stretchable fibers

S. Zokaei, M. Craighero, L. M. Kneissl, R. Kroon, A. Lund, C. Müller
Department of Chemistry and Chemical Engineering
Chalmers University of Technology
Göteborg 41296, Sweden
E-mail: anja.lund@chalmers.se; christian.muller@chalmers.se
C. Cea, D. Khodagholy
Department of Electrical Engineering
School of Engineering and Applied Science
Columbia University
New York, NY 10027, USA

The ORCID identification number(s) for the author(s) of this article can be found under https://doi.org/10.1002/smll.202102813.

DOI: 10.1002/smll.202102813

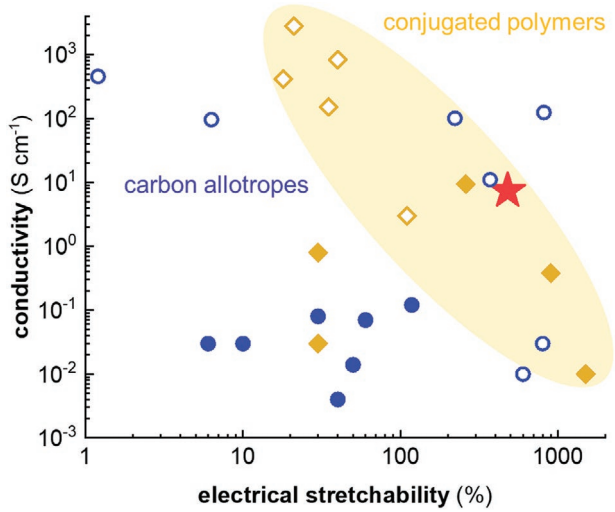

Figure 1. Ashby plot of the electrical conductivity versus electrical stretchability, that is, the maximum strain at which a fiber remains conducting, for fibers manufactured by blending or compounding conjugated polymers (filled yellow diamonds) or conductive carbon allotropes (blue filled circles) with an insulating polymer matrix, and for fibers manufactured by other methods such as coating or in situ polymerization of the conductive polymer (empty diamonds) or conductive carbon allotropes (empty circles) on the surface of an insulating textile fiber. The data were obtained from refs. [26,29,32,33,36–53] and from the present work (red star).

composed of polymers or carbon allotropes as the conducting material display values of ε_e ranging from 1.2% to 1500% and σ from 0.004 to 2800 S cm^{-1} (**Figure 1**). Note that in case of some conducting fibers there is a considerable increase in resistance upon stretching.[29,36,37]

To date, only a handful of studies are available where polymers constitute the conducting component of a conducting fiber with a high electrical stretchability of $\varepsilon_e > 200\%$. Polyurethane (PU) and polyesters are the most commonly used elastomers in conductive blend fibers with PEDOT:PSS,[29,54] polyaniline (PANI),[38] or polypyrrole[55] as the conductive constituent. Also, the combination of a styrenic copolymer with poly(3-hexylthiophene) (P3HT) has resulted in conductive fibers with ε_e up to 900%.[39,40] Conductive polymeric fibers fabricated via blending tend to permit a higher span of applied strain compared to neat conducting polymer fibers or those fabricated by other means (cf. Figure 1). We postulate that the high Young's modulus and inherent brittleness of many conjugated polymers is the underlying reason why it has been challenging to produce stretchable fibers with these materials. Conjugated polymers tend to be stiff and brittle due to a low molecular weight and a strong tendency for π–π stacking of their backbone, which on the other hand is desired because it tends to yield a high charge-carrier mobility.[25,56] As a result, conjugated polymers typically feature a Young's modulus in the range of a few 100 MPa to several GPa at room temperature.[57–59] An additional challenge arises if doping of the conjugated polymer is carried out, which is needed to render the material electrically conducting. In particular co-processing of the polymer together with dopant molecules can lead to premature aggregation, which tends to yield a brittle solid.[60,61]

The use of conjugated polymers with oligoethylene glycol side chains would offer an intriguing alternative because, in their pristine form, they tend to be exceedingly soft.[62] These materials are attractive for a wide range of applications such as bioelectronics,[63–66] energy harvesting,[67–71] and energy storage,[72–74] thanks to their ability to transport and store electronic charges, facilitated by the conjugated backbone, as well as ions, the affinity for which is greatly enhanced by polar side chains. Oligoethylene glycol side chains bestow the polymer with a sub-zero glass transition temperature T_g and, at room temperature, a low Young's modulus,[62,75] which however means that these polymers display limited mechanical integrity. Conversely, the polarity of these polymers enables mixing with polar components such as PU.

In this study, we introduce a strategy to utilize the softness and electrical properties of a polythiophene with tetraethylene glycol side chains (p($g_4$2T-T); cf. **Figure 2** for chemical structure). We blend p($g_4$2T-T) with elastomeric PU and use this semiconductor:insulator blend to prepare stretchable electrically conducting fibers with diameters of 30 to 70 µm through wet-spinning and subsequent chemical doping with iron(III) p-toluenesulfonate hexahydrate (Fe(Tos)$_3\cdot 6H_2O$). The doped fibers display a conductivity of up to 7.4 S cm^{-1} and remain conducting until fracture at 480% strain (the resistance increased by a factor of only 2–4 times), which places them among the best performing stretchable fibers that have been reported to date and represents a record combination of properties for conjugated polymer-based fibers (Figure 1). Importantly, they retain their electrical and elastomeric properties during several hundred strain cycles with a maximum strain of $\varepsilon = 50\%$ and display a promising stability at ambient conditions for at least 12 months.

2. Results and Discussion

2.1. Wet Spinning

During wet spinning of polymer fibers, the constituent polymers are first dissolved and then extruded into a coagulation bath. The coagulation bath consists of a solvent that is miscible with the first solvent but does not dissolve the polymer. The fibers gradually solidify in the coagulation bath, before being collected and wound onto a bobbin. Both p($g_4$2T-T) and the here used polycarbonate-based PU could be readily dissolved in dimethyl formamide (DMF) even at the required high concentrations of 50–70 g L^{-1}. To prepare blend fibers, polymer solutions (with the same concentrations) were mixed at a ratio of 1:4 p($g_4$2T-T):PU and then extruded at an extrusion rate $v_{extrusion}$ through a fine needle into a coagulation bath consisting of deionized water and isopropanol (IPA) (Figure 2a). The fibers were pulled through the coagulation bath and collected by a take-up roller at a certain rate $v_{take\text{-}up}$. After collection, the fibers were washed in acetonitrile (AcN) and/or water to remove any remaining solvent.

The cross section and microstructure of wet spun fibers are a result of multiple diffusion processes that take place in the coagulation bath, each one a result of the interactions between solvents and polymers, and of the timescale as determined by the processing parameters. We found that our first batches of PU fibers, spun from a polymer solution of 50 g L^{-1} into a coagulation bath of 1:3 IPA:water (extrusion rate 3 mL h^{-1}, 27 G needle) had a flattened cross section indicating insufficient

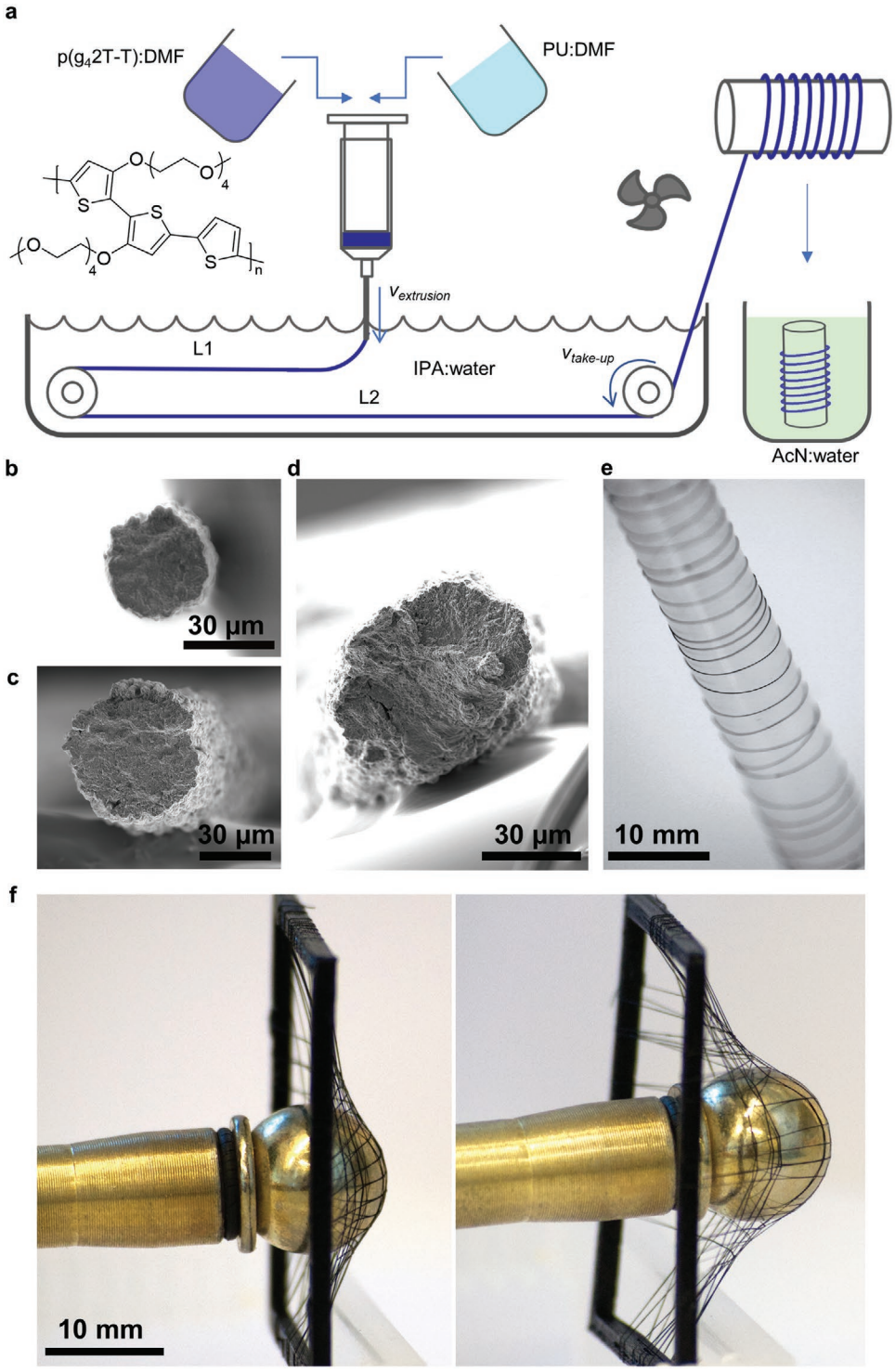

Figure 2. a) Schematic of the wet spinning process. Solutions of p($g_4$2T-T) and PU in DMF are mixed in a syringe and then injected into a coagulation bath through a thin needle. The extruded fiber gradually solidifies along the spin line in the coagulation bath, whereafter it is collected by a take-up roller. A fan is used to speed up drying process of fibers. After collection, the fibers are immersed into water and/or AcN, to ensure complete removal of DMF. SEM micrographs of the cross sections of p($g_4$2T-T):PU fibers: b) F_{thin}, c) F_{thick}, and d) F_{midi}; e) photograph of a roll of p($g_4$2T-T):PU fiber; f) hand-made weave composed of p($g_4$2T-T):PU fibers that can undergo reversible deformation.

coagulation in the spin line. By adjusting the concentration of IPA in the coagulation bath from 25% to 50% we could improve the fiber cross section from flat to semi-circular (Figure S1, Supporting Information). A further increase of the IPA content to 60–70% increased the spin-line stability and allowed us to produce continuous p($g_4$2T-T):PU fibers, referred

Table 1. Wet-spinning parameters: polymer concentration in the spinning dope c, spin-line path lengths in the coagulation bath (L_1:L_2) (cf. Figure 2), coagulation bath ratio of IPA to water, extrusion rate $\nu_{extrusion}$, needle gauge G, take-up rate $\nu_{take\text{-}up}$, rinsing time in AcN and then water t_{rinse}, and the resulting cross-sectional area A of PU and p($g_4$2T-T):PU fibers.

Fiber	c [g L^{-1}]	L_1:L_2 [cm:cm]	IPA:water	$\nu_{extrusion}$ [mL h^{-1}]	G	$\nu_{take\text{-}up}$ [mm s^{-1}]	t_{rinse} [min:min]	A [μm^2]
PU_{thin}	50	0:60	60:40	2	27 G	20	0:20	780 ± 75
F_{thin}	50	0:60	60:40	2	23 G	20–28	0:20	740 ± 44
F_{midi}	50	30:60	70:30	3.5	23 G	20	3:10	2874 ± 559
PU_{thick}	70	30:60	70:30	3.5–4	23 G	23	3:10	3650 ± 327
F_{thick}	70	30:60	70:30	3.5–4	23 G	20–23	3:10	3814 ± 413

to as F_{thin}, at an extrusion rate of 2 mL h^{-1}. The F_{thin} fibers displayed a round cross section area (≈740 μm^2) with a diameter of ≈30 μm and a textured surface (Figure 2b, **Table 1**). For reference, pure PU fibers (PU_{thin}) were prepared using the same parameters. Next, in order to modify the fiber thickness, we increased the extrusion rate together with the spin-line path length while keeping a similar take-up speed and used a larger 23 G needle/spinneret. Clearly, an increased length of the spin-line path inside the coagulation bath improved the removal of DMF prior to collection, thus preventing the fiber from flattening on the take-up roller. This process resulted in circular/semi-circular fibers, denoted F_{midi}, with a diameter of ≈60 μm and an average cross-sectional area of ≈2870 μm^2 (Figure 2d, Table 1). By further increasing the polymer solution concentration to 70 g L^{-1}, we could prepare thicker fibers, referred to as F_{thick}, with a diameter of ≈70 μm and a cross-sectional area of ≈3810 μm^2 (Figure 2c, Table 1; see Figure S2, Supporting Information for an overview of the employed processing parameters). We found the spinning process to be very stable and could, for a given set of process parameters, repeatedly prepare fibers with the same characteristics. Limited by the amount p($g_4$2T-T), we produced ≈5 m of continuous filament during each spinning experiment. The fibers (Figure 2e) could be readily incorporated into a hand-made weave, which deforms reversibly (Figure 2f).

2.2. Chemical Doping Imparts Electrical Conductivity with Retained Mechanical Properties

For an initial assessment of the electrical conductivity of our fibers, we used the model dopant 2,3,5,6-tetrafluoro-7,7,8,8-tetracyanoquinodimethane (F4TCNQ) (see **Figure 3**a for chemical structure) dissolved in AcN or diethyl ether (Et_2O) at 1 g L^{-1}. A bobbin with F_{thin} fibers was submerged in the dopant solution for 24 h (Figure 3b), resulting in conductivities of ≈2.4 S cm^{-1} (AcN) and ≈7.5 S cm^{-1} (Et_2O) (**Table 2**; Table S1, Figure S3, Supporting Information).

For wearable applications, it is of outmost importance that the materials are stable and non-toxic. As F4TCNQ is inherently toxic and moreover tends to sublime over time,[75,76] we proceeded to evaluate alternative dopants that allow us to produce conducting fibers with long-term stability in terms of both, electrical and mechanical properties. We chose to evaluate two acid dopants: dodecylbenzenesulfonic acid (DBSA) and 4-ethylbenzene sulfonic acid (EBSA)—which have been shown to strongly dope p($g_4$2T-T)[77]—as well as $Fe(Tos)_3 \cdot 6H_2O$ (chemical structures and doping scheme in Figure 3a,b). We have previously argued that doping with DBSA or EBSA entails an acid mediated oxidation of the polymer through oxygen.[77] $Fe(Tos)_3 \cdot 6H_2O$ instead directly oxidizes p($g_4$2T-T) leading to the formation of iron(II) p-toluenesulfonate, $Fe(Tos)_2$, while the third p-toluenesulfonate anion becomes the negative counterion for the positive polaron on the p($g_4$2T-T) backbone. As doping of bulk materials is a diffusion limited process,[78] we used long doping times by immersing F_{thin} fibers in dopant solutions (AcN or Et_2O) for 1 to 48 h. For a given dopant:solvent system the degree of doping that can be achieved depends on a number of parameters such as the extent to which the solvent swells the respective fiber, the solubility of the dopant as well as its miscibility with the polymer. We chose to work with AcN and Et_2O because they readily dissolve the studied dopants and likely lead to swelling of the polar conjugated polymer. A doping time of up to 48 h was chosen because previous studies have shown that this time is sufficient to evenly dope 40 μm thick P3HT films with F4TCNQ or with a molybdenum dithiolene complex.[58] Fibers doped with EBSA, DBSA, or $Fe(Tos)_3 \cdot 6H_2O$ displayed a conductivity between 0.2 and 7.4 S cm^{-1}, depending on the choice of dopant, doping time, and type of solvent (Table 2, Figure 3c; Table S1, Figure S2, Supporting Information). We obtained the highest value after 24 h of doping F_{midi} with $Fe(Tos)_3 \cdot 6H_2O$ in AcN (Table 2).

Doping can alter the mechanical properties of conjugated polymers, as for instance observed in case of poly(3-alkylthiophene) fibers doped with $FeCl_3$, which became stiffer upon doping.[79,80] We were curious about the impact of doping on our blend fibers and carried out tensile tests of both undoped and doped F_{thin} fibers. We found that the addition of p($g_4$2T-T) to PU resulted in a reduction of the Young's modulus from 44 to 19 MPa (Figure 3d, Table 2). After doping for 1–4 h the blend fibers display an increase in stiffness to 60 MPa, while further doping for 24 or 48 h yields a slightly lower value of $E \approx 33$ MPa (Figure 3d, Table 2). Wide-angle X-ray scattering (WAXS) indicates that the PU component is largely amorphous, resulting in a broad halo centered around 1.6 Å^{-1} (Figure 3e; Figure S4, Supporting Information). Upon addition of p($g_4$2T-T) to PU (F_{midi}) a peak emerges at 0.34 Å^{-1}, which we assign to lamellar stacking of the conjugated polymer. After doping, this peak shifts to 0.26 Å^{-1} and its relative intensity increases, and a new peak at around 1.81 Å^{-1} appears, indicative of π–π stacking,[75,77] which may explain the observed increase in the Young's modulus of the blend fibers. Further, we note that WAXS diffractograms of doped fibers do not show any scattering peaks reminiscent of undoped material, that is, we only see a single peak at 0.26 Å^{-1}, which indicates that the full volume of the fibers

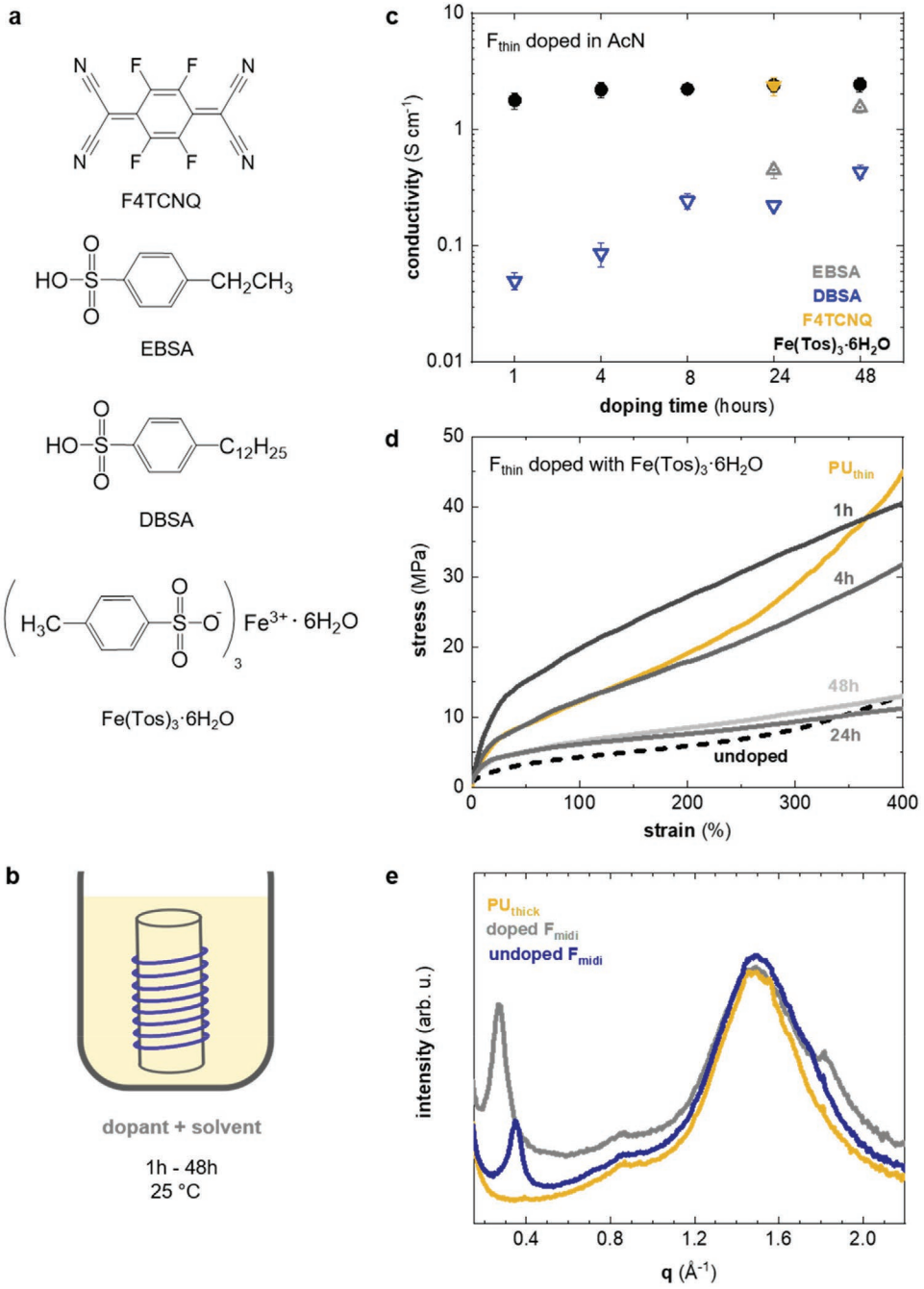

Figure 3. a) Chemical structures of the used dopants starting from top: F4TCNQ, EBSA, DBSA, and $Fe(Tos)_3{\cdot}6H_2O$; b) a schematic illustration of the doping procedure, where a roll of the spun fibers was immersed in a solution of the dopant; c) electrical conductivity of p($g_4$2T-T):PU fibers doped with $Fe(Tos)_3{\cdot}6H_2O$ (black filled circles), F4TCNQ (yellow filled triangle), DBSA (blue triangles), and EBSA (grey triangles) in AcN as a function of doping time; d) tensile stress/strain curves up to 400% strain of wet-spun PU fibers (PU_{thin}) (yellow solid line), p($g_4$2T-T):PU fibers (F_{thin}) before (black dashed line) and after doping with $Fe(Tos)_3{\cdot}6H_2O$ for different times (dark to light grey solid lines). None of the fibers broke during this test; e) transmission WAXS spectra of PU fibers (PU_{thick}) (yellow line) and p($g_4$2T-T):PU fibers (F_{midi}) before (blue line) and after doping with $Fe(Tos)_3{\cdot}6H_2O$ for 24 h (grey line).

is doped. Longer doping times result in a further uptake of dopant molecules and likely start to disrupt the nanostructure of the polymer, which may explain the slight decrease in stiffness. We chose to dope fibers with $Fe(Tos)_3{\cdot}6H_2O$ in AcN for 24 h for all further experiments.

2.3. Electrical Stretchability and Long-Term Stability

The wet spun p($g_4$2T-T):PU fibers F_{midi} exhibit a strain at break ε_b = 440% before doping (i.e., about half of that of wet spun PU fibers; ε_b = 800% cf. Figure S5, Supporting Information),

Table 2. Dopant, doping time in AcN dopant solutions t_{doping}, electrical conductivity σ (measured on m samples), Young's modulus E (measured on n samples) of PU and p($g_4$2T-T):PU fibers ($n = 2$ for some doped fibers because only a limited amount of material was prepared). The fibers $F_{midi,9m}$ were characterized 9 months after spinning and doping, during which time they were stored at room temperature in air. n.a. = not applicable. Errors were calculated according to $\Delta x = (x_{max} - x_{min}) / (2\sqrt{n})$.

Fiber	Dopant	t_{doping} [h]	σ [S cm^{-1}]	m	E [MPa]	n
PU_{thin}	n.a.	n.a.	n.a.	n.a.	44 ± 6	4
F_{thin}	Undoped	n.a.	n.a.	n.a.	19 ± 3	5
	F4TCNQ	24	2.4 ± 0.4	5	26 ± 2	3
	DBSA	24	0.2 ± 0.1	5	27 ± 1	3
	EBSA	24	0.4 ± 0.1	4	30 ± 2	2
	$Fe(Tos)_3{\cdot}6H_2O$	1	1.8 ± 0.3	5	58 ± 6	2
	$Fe(Tos)_3{\cdot}6H_2O$	4	2.2 ± 0.3	5	60 ± 6	3
	$Fe(Tos)_3{\cdot}6H_2O$	24	2.4 ± 0.3	4	33 ± 1	2
	$Fe(Tos)_3{\cdot}6H_2O$	48	2.4 ± 0.3	4	33 ± 7	6
F_{midi}	Undoped	n.a.	n.a.	n.a.	19 ± 1	3
	$Fe(Tos)_3{\cdot}6H_2O$	24	7.4 ± 0.8	4	32 ± 6	3
$F_{midi,9m}$	$Fe(Tos)_3{\cdot}6H_2O$	24	4.0 ± 0.4	4	31 ± 1	2
F_{thick}	Undoped	n.a.	n.a.	n.a.	22 ± 2	11
	$Fe(Tos)_3{\cdot}6H_2O$	24	2.9 ± 0.6	15	23 ± 1	2

which remains unchanged after doping (ε_b = 480%, **Figure 4**a, left; Figure S5, Supporting Information, top). We repeated this experiment with $F_{midi,9m}$ fibers, that had been stored at room temperature in air over 9 months after spinning and doping, and found that their mechanical properties remain largely unaffected with an ε_b = 435% and E = 31 MPa (Figure 4a, right; Figure S5, Supporting Information, top). Further, we repeatedly characterized the electrical conductivity of the doped fibers during long term storage at ambient conditions. We found that aside from a reduction during the first month after doping, the conductivity of the doped blend fibers is stable for at least 12 months (Figure 4b). In conclusion, the fibers display a high degree of stability in terms of both, electrical and mechanical characteristics.

To further study the usefulness of our material for the design of stretchable devices, we characterized their electrical stretchability.[25] First, we recorded the electrical resistance R during tensile tests of doped F_{midi} and F_{thick} fibers (Figure 4a; Figure S6, Supporting Information). We found that the normalized resistance $R_n = R/R_0$, where R_0 is the resistance at the start of the test, remains largely unaffected up to nearly 300% strain. Notably, the F_{midi} fibers remain conducting until they break at around 480%. The electrical stretchability is unchanged even after long term ambient storage, as demonstrated by the characterization of $F_{midi,9m}$ fibers (Figure 4a, right).

We went on to investigate the degree of elastic recovery of the fibers after tensile deformation. A single fiber (F_{midi}) was stretched to a strain ε_m and then relaxed for 30 s, followed by another stretch cycle to a higher ε_m (**Figure 5**a, top). The 30 s relaxation time allowed the fiber to relax to a strain ε_r, and the elastic recovery was taken as $(\varepsilon_m - \varepsilon_r)/\varepsilon_r$. We find that the elastic recovery for the doped p($g_4$2T-T):PU fiber does not significantly differ from that of the PU fiber, until $\varepsilon_m \geq 50\%$ (Figure 5a; Figure S7a, Supporting Information). Notably, $F_{midi,9m}$ fibers display the same elastic recovery (Figure 5a, bottom; Figure S7b, Supporting Information). We proceeded to subject the conducting fiber, F_{thick}, to cyclic stretching where the fiber was stretched to 50% strain and then allowed to relax for 30 s, for > 400 cycles (Figure 5b, top; Figure S8, Supporting Information). We chose to focus on cyclic stretching experiments with a maximum strain of 50% because of the high degree of elastic recovery up to this strain (see Figure 5a). The electrical resistance was recorded in situ and we observe that during each strain cycle, the resistance initially increases slightly and then reverts to its initial value R_0. After 442 strain cycles $R \approx 0.9\ R_0$ (Figure 5b, top). The force required to stretch the fiber is 4 to 5 mN throughout the test, indicating an absence of stress softening. We conclude that the blend fiber has a high electrical and mechanical cyclic stability (Figure 5b, bottom).

The here developed scalable production process of stretchable p($g_4$2T-T):PU fibers allowed us to prepare a directional triangular strain sensor device (**Figure 6**a). We utilized doped F_{thick} fibers to construct a 5 mm equilateral triangle around 3 Au-coated pins that were mounted on a linear manipulator to allow precise control of motion on a defined corner. The sides of the triangle consisted of our stretchable fibers, and the movement of a corner pin results in mechanical strain and change in electrical resistance of the two adjacent fibers sections, while the opposite fiber section will remain unchanged. This configuration enables us to define the direction and magnitude of strain by identifying the fibers and their resistance modulation, respectively. Next, we measured the resistance changes ΔR of the fiber with respect to the deformation of the triangle due to external force. We found that ΔR is consistently proportional to the expansion length of the triangle, over multiple stretches (Figure 6b). Furthermore, the fiber on the opposite side of the triangle retained its resistance value, allowing us to determine the direction of the strain. The normalized response ($\Delta R/R_0$) was linear up to 120% strain, providing an effective means to accurately determine the magnitude of the strain

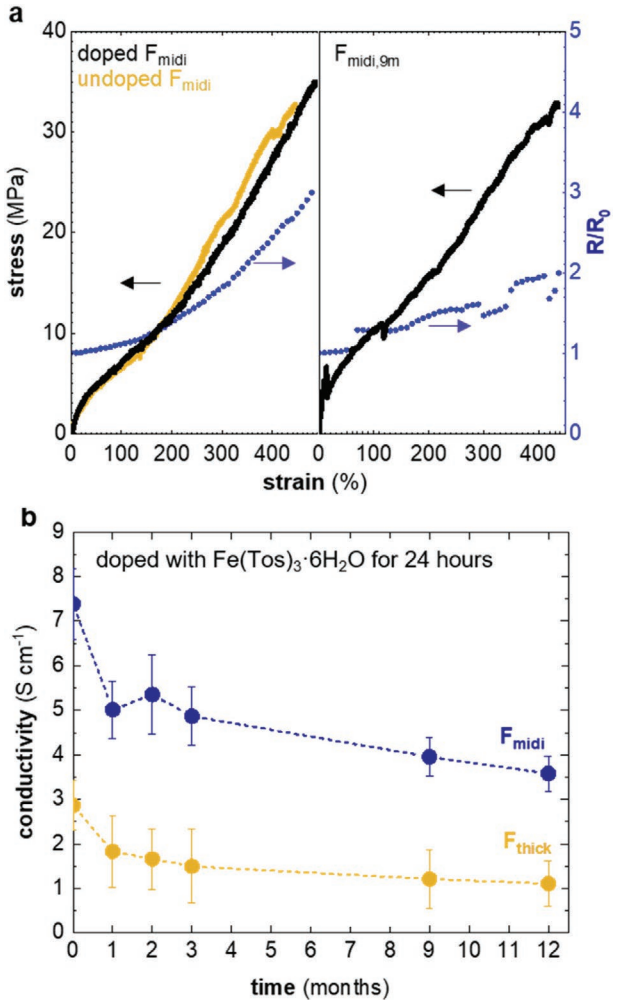

Figure 4. a) Stress/strain tensile deformation curves of p($g_4$2T-T):PU fiber F_{midi} (left) before (yellow line) and after doping with $Fe(Tos)_3 \cdot 6H_2O$ (black line) and (right) $F_{midi,9m}$ that are characterized 9 months after doping, during which time they were stored at room temperature in air (black line). Fibers were stretched until breakage. In situ recorded change in electrical resistance R/R_0 (blue symbols) where R_0 is the resistance of the fiber prior to the test; b) electrical conductivity of doped p($g_4$2T-T):PU fibers F_{midi} (blue symbols) and F_{thick} (yellow symbols) measured repeatedly during storage at room temperature in air for up to 12 months.

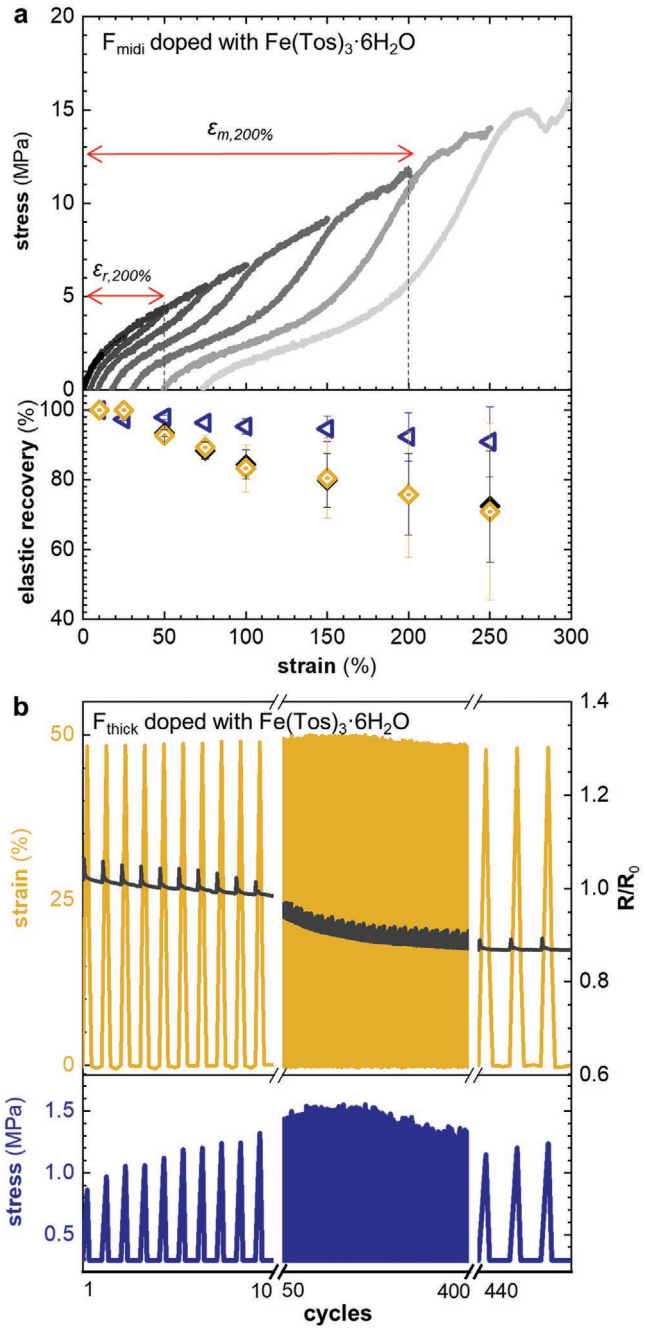

Figure 5. a) (Top) Stress/strain data collected during a series of consecutive tensile deformation experiments where a p($g_4$2T-T):PU fiber (F_{midi}) doped with $Fe(Tos)_3 \cdot 6H_2O$ was stretched to a maximum strain ε_m and then relaxed for 30 s, followed by another stretch cycle to a higher ε_m. After each stretch cycle, the fiber relaxes to a strain ε_r. As an example, the red arrows indicate the ε_m and ε_r for the ε_m = 200% cycle. (Bottom) Elastic recovery $(\varepsilon_m - \varepsilon_r)/\varepsilon_r$ for a p($g_4$2T-T):PU fiber (F_{midi}) doped with $Fe(Tos)_3 \cdot 6H_2O$ recorded shortly after doping (yellow diamonds), after doping and 9 months storage at room temperature in air (black diamonds), and for the PU fiber (PU_{thick}) (blue triangles); b) cyclic strain testing of the p($g_4$2T-T):PU fiber (F_{thick}) doped with $Fe(Tos)_3 \cdot 6H_2O$ stretched to 50% then released for 30 s (top, yellow line), in situ recorded change in electrical resistance R/R_0, where R_0 is the initial resistance (top, grey line), and the applied force during the 442 strain cycles (bottom, blue line).

while maintaining a negligible response for the opposing fiber (Figure 6c). The linear increase in $\Delta R/R_0$ indicates that the performance of the device is reproducible both within the region up to 50% strain where close to full elastic recovery takes place (see Figure 5a) as well as at larger strains up to at least 120% strain.

3. Conclusions

We have presented wet spun blend fibers of p($g_4$2T-T) and PU which display both mechanical and electrical stretchability of up to 480% after doping with iron(III) p-toluenesulfonate hexahydrate ($Fe(Tos)_3 \cdot 6H_2O$). The fibers are reversibly stretchable up to a strain of 50%, revealing elastomeric behavior of the

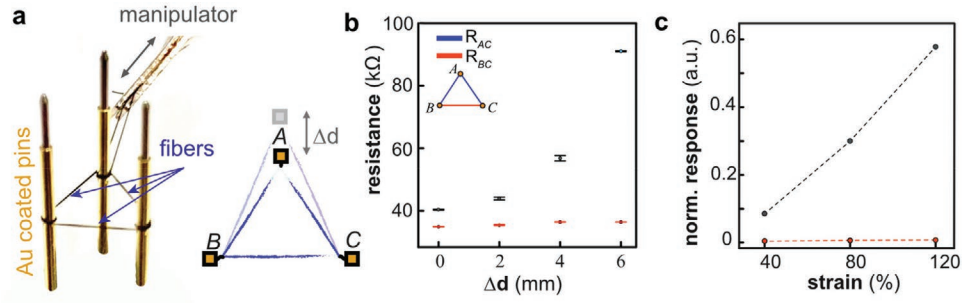

Figure 6. a) Photograph of the directional strain sensor based on fiber F_{thick} doped with $Fe(Tos)_3{\cdot}6H_2O$ (left). Schematic of the sensor illustrating stretched adjacent fibers (*AB*, *AC*) with intact opposing fiber (*BC*) during an external strain applied to point *A* (right); b) modulation of fiber resistance as a function of positional change of corner pin *A*; c) normalized response of the fibers (change in resistance per initial resistance, $\Delta R/R_0$), demonstrating a linear response up to a strain of 120%.

fibers. Our doped fibers with maximum conductivity of 7.4 S cm^{-1} display excellent stability in terms of both mechanical and electrical properties, even after prolonged storage under ambient conditions. We conclude that blending soft polar polythiophenes with elastomers such as PU is a promising and straight-forward strategy to improve both the stretchability and the degree of elastic recovery of these polymers.

4. Experimental Section

Materials: The synthesis of p($g_4$2T-T) ($M_n \approx 24$ kg mol^{-1}; PDI ≈ 3.3) was described elsewhere.[75] The polymer was dried for 20 h at 40 °C under vacuum before use. ChronoFlex C, a polycarbonate-based PU, was obtained from AdvanSource Biomaterials, USA and dried for 4 h at 80 °C under vacuum prior to use. Anhydrous AcN was purchased from Acros Organics. DMF, IPA, anhydrous diethyl ether (Et_2O), iron(III) p-toluenesulfonate hexahydrate ($Fe(Tos)_3{\cdot}6H_2O$), DBSA, and EBSA were purchased from Sigma Aldrich. F4TCNQ was purchased from TCI chemicals. DMF was purified with a MB-SPS 800 solvent purification system (MBraun, Germany). All dopants were used as received.

Wet Spinning: p($g_4$2T-T) and PU were dissolved in degassed and dried (over activated 4 Å molsieves) DMF at concentrations of 50 and 70 g L^{-1} (cf. Table 1) at 25 and 90 °C, respectively. After purging with nitrogen for a few minutes, the PU solution was mixed with the equivalent solution of p($g_4$2T-T) at a ratio of 4:1. The pure PU and blend solutions were injected through a thin-walled B Braun needle with a 27 G (outer diameter = 0.4 mm) or 23 G (outer diameter = 0.6 mm) blunt tip, into a coagulation bath consisting of IPA and deionized water. The injection rate was controlled by a syringe pump (Harvard Apparatus Inc., USA) set to different extrusion speeds $v_{extrusion}$ in the range of 2 to 4 mL h^{-1}. The speed of a custom-built DC-motorized take-up roller (diameter = 25 mm) was controlled by the output voltage from a power supply (EL302RT from Aim-TTi). The take-up speed $v_{take\text{-}up}$ was kept in the range of 20–26 mm s^{-1}. The spun fibers were rinsed in deionized water and AcN separately (see Table 1).

Scanning Electron Microscopy: Samples for scanning electron microscopy (SEM) were freeze-fractured in liquid nitrogen, and then sputtered with palladium. SEM imaging was done with a JSM-7800F (JEOL Ltd., Japan) or LEO Ultra 55 (Zeiss, Germany) at an acceleration voltage of 2–3 kV. The fiber diameter was estimated using ImageJ.

Doping and Electrical Characterization: Blend fibers rolled onto a small bobbin were doped by submersion into dopant solutions of F4TCNQ, $Fe(Tos)_3{\cdot}6H_2O$, EBSA, or DBSA in AcN or Et_2O (1 g L^{-1}) for the specified time (1 to 48 h). Fibers F_{midi} and F_{thick} were subsequently rinsed in AcN for 1 min. For characterization of the electrical conductivity, samples of the doped blend fibers were placed on a glass substrate whereafter silver paint (fast drying silver suspension, Agar scientific Ltd.) was applied on top to form contact points at 10 mm spacing. The resistance of each 10 mm section was measured using a U1253B handheld multimeter in 2-point configuration (Keysight Technologies). The electrical contact resistance R_c of the authors' 2-point probe setup was estimated by a transmission line measurement, that is, the electrical resistance was plotted as a function of section length and then extrapolated to zero length. It was found that $R_c \approx 0.1R_m$ where R_m is the measured resistance and corrected the resistance according to $R = R_m - R_c$. The electrical conductivity was then calculated using the average fiber cross section area *A* as observed by SEM according to $\sigma = l/(R \cdot A)$ where *l* is the length of the characterized fiber section.

Mechanical Testing: Tensile testing up to 400% strain and cyclic strain tests were performed using a DMA Q800 (TA Instruments) in controlled force mode at a rate of 0.005 N min^{-1} with a preload force of 0.0005 N. Tensile tests to break and elastic recovery characterization were carried out on an Instron tensile tester equipped with a 10 N load cell at 10 mm min^{-1} strain rate and 10 mm gauge length. Elastic recovery tests were performed by stretching to ε_m, then releasing for 30 s by reverting to initial gauge length, followed by subsequent stretch to a larger ε_m (10% ≤ ε_m ≤ 300%). Cyclic strain tests were performed on the blend fibers by applying 50% strain followed by a 30 s release. The first 10 cycles (Figure S7, Supporting Information) were regarded as a conditioning step and therefore not included in the final results. Silver paint and copper tape were applied to the fiber ends, to aid the electrical connection via probes to a Keysight U1253B multimeter, which monitored electrical resistance during the strain cycles, tensile, and elastic recovery tests.

Strain Sensing: Strain sensing tests were carried out using an in-house setup consisting of 3 Au-coated pins, which constitute the corners of an equilateral triangle (length of each side = 5 mm) fixed on a linear manipulator, enabling control over the strain by translating one of the corners. Fibers were connected to the pins using conducting silver paste. The change in resistance of the fiber upon stretching two sides of the triangle was monitored using a source measure unit.

Supporting Information

Supporting Information is available from the Wiley Online Library or from the author.

Acknowledgements

The authors gratefully acknowledge financial support from the European Research Council (ERC) under grant agreement no. 637624 and the Knut and Alice Wallenberg Foundation through a Wallenberg Academy Fellows Prolongation grant. WAXS measurements and electron microscopy were performed at the Chalmers Material Analysis Laboratory (CMAL).

The authors thank Anders Mårtensson for help with scanning electron microscopy imaging of the fibers.

Conflict of Interest

The authors declare no conflict of interest.

Data Availability Statement

The data that support the findings of this study are available from the corresponding author upon reasonable request.

Keywords

conjugated polymers, elastomer fibers, electrical stretchability, electronic textiles, polyurethane

Received: June 10, 2021
Revised: August 24, 2021
Published online:

[1] T. R. Ray, J. Choi, A. J. Bandodkar, S. Krishnan, P. Gutruf, L. Tian, R. Ghaffari, J. A. Rogers, *Chem. Rev.* **2019**, *119*, 5461.
[2] H. Yuk, B. Lu, X. Zhao, *Chem. Soc. Rev.* **2019**, *48*, 1642.
[3] M. Kaltenbrunner, T. Sekitani, J. Reeder, T. Yokota, K. Kuribara, T. Tokuhara, M. Drack, R. Schwödiauer, I. Graz, S. Bauer-Gogonea, S. Bauer, T. Someya, *Nature* **2013**, *499*, 458.
[4] T. Someya, Z. Bao, G. G. Malliaras, *Nature* **2016**, *540*, 379.
[5] J. Park, J. Kim, S.-Y. Kim, W. H. Cheong, J. Jang, Y.-G. Park, K. Na, Y.-T. Kim, J. H. Heo, C. Y. Lee, J. H. Lee, F. Bien, J.-U. Park, *Sci. Adv.* **2018**, *4*, eaap9841.
[6] D. H. Keum, S.-K. Kim, J. Koo, G.-H. Lee, C. Jeon, J. W. Mok, B. H. Mun, K. J. Lee, E. Kamrani, C.-K. Joo, S. Shin, J.-Y. Sim, D. Myung, S. H. Yun, Z. Bao, S. K. Hahn, *Sci. Adv.* **2020**, *6*, eaba3252.
[7] Z. He, G. Zhou, J.-H. Byun, S.-K. Lee, M.-K. Um, B. Park, T. Kim, S. B. Lee, T.-W. Chou, *Nanoscale* **2019**, *11*, 5884.
[8] M. Liu, X. Pu, C. Jiang, T. Liu, X. Huang, L. Chen, C. Du, J. Sun, W. Hu, Z. L. Wang, *Adv. Mater.* **2017**, *29*, 1703700.
[9] W. Fan, Q. He, K. Meng, X. Tan, Z. Zhou, G. Zhang, J. Yang, Z. L. Wang, *Sci. Adv.* **2020**, *6*, eaay2840.
[10] M. Tessarolo, I. Gualandi, B. Fraboni, *Adv. Mater. Technol.* **2018**, *3*, 1700310.
[11] J. Di, X. Zhang, Z. Yong, Y. Zhang, D. Li, R. Li, Q. Li, *Adv. Mater.* **2016**, *28*, 10529.
[12] J. A. Lee, A. E. Aliev, J. S. Bykova, M. J. de Andrade, D. Kim, H. J. Sim, X. Lepró, A. A. Zakhidov, J.-B. Lee, G. M. Spinks, S. Roth, S. J. Kim, R. H. Baughman, *Adv. Mater.* **2016**, *28*, 5038.
[13] J. Y. Oh, D. Son, T. Katsumata, Y. Lee, Y. Kim, J. Lopez, H. C. Wu, J. Kang, J. Park, X. Gu, J. Mun, N. G. Wang, Y. Yin, W. Cai, Y. Yun, J. B. Tok, Z. Bao, *Sci. Adv.* **2019**, *5*, eaav3097.
[14] T. Yamada, Y. Hayamizu, Y. Yamamoto, Y. Yomogida, A. Izadi-Najafabadi, D. N. Futaba, K. Hata, *Nat. Nanotechnol.* **2011**, *6*, 296.
[15] F. H. Silver, J. W. Freeman, D. DeVore, *Skin Res. Technol.* **2001**, *7*, 18.
[16] M. F. Ashby, *Materials and the Environment*, 2nd ed., Butterworth-Heinemann, Boston **2013**.
[17] Y. Kim, J. Zhu, B. Yeom, M. Di Prima, X. Su, J.-G. Kim, S. J. Yoo, C. Uher, N. A. Kotov, *Nature* **2013**, *500*, 59.
[18] S. Choi, S. I. Han, D. Jung, H. J. Hwang, C. Lim, S. Bae, O. K. Park, C. M. Tschabrunn, M. Lee, S. Y. Bae, J. W. Yu, J. H. Ryu, S.-W. Lee, K. Park, P. M. Kang, W. B. Lee, R. Nezafat, T. Hyeon, D.-H. Kim, *Nat. Nanotechnol.* **2018**, *13*, 1048.
[19] H. Sun, Z. Han, N. Willenbacher, *ACS Appl. Mater. Interfaces* **2019**, *11*, 38092.
[20] P. J. Taroni, G. Santagiuliana, K. Wan, P. Calado, M. Qiu, H. Zhang, N. M. Pugno, M. Palma, N. Stingelin-Stutzman, M. Heeney, O. Fenwick, M. Baxendale, E. Bilotti, *Adv. Funct. Mater.* **2018**, *28*, 1704285.
[21] N. Kim, S. Lienemann, I. Petsagkourakis, D. Alemu Mengistie, S. Kee, T. Ederth, V. Gueskine, P. Leclère, R. Lazzaroni, X. Crispin, K. Tybrandt, *Nat. Commun.* **2020**, *11*, 1424.
[22] T. S. Hansen, K. West, O. Hassager, N. B. Larsen, *Adv. Funct. Mater.* **2007**, *17*, 3069.
[23] Y. Wang, C. Zhu, R. Pfattner, H. Yan, L. Jin, S. Chen, F. Molina-Lopez, F. Lissel, J. Liu, N. I. Rabiah, Z. Chen, J. W. Chung, C. Linder, M. F. Toney, B. Murmann, Z. Bao, *Sci. Adv.* **2017**, *3*, e1602076.
[24] A. Lund, N. M. van der Velden, N.-K. Persson, M. M. Hamedi, C. Müller, *Mater. Sci. Eng. R Rep.* **2018**, *126*, 1.
[25] G.-J. N. Wang, A. Gasperini, Z. Bao, *Adv. Electron. Mater.* **2018**, *4*, 1700429.
[26] E. Bilotti, R. Zhang, H. Deng, M. Baxendale, T. Peijs, *J. Mater. Chem.* **2010**, *20*, 9449.
[27] Y. Lu, J. Jiang, S. Yoon, K.-S. Kim, J.-H. Kim, S. Park, S.-H. Kim, L. Piao, *ACS Appl. Mater. Interfaces* **2018**, *10*, 2093.
[28] S. Lee, S. Shin, S. Lee, J. Seo, J. Lee, S. Son, H. J. Cho, H. Algadi, S. Al-Sayari, D. E. Kim, T. Lee, *Adv. Funct. Mater.* **2015**, *25*, 3114.
[29] M. Z. Seyedin, J. M. Razal, P. C. Innis, G. G. Wallace, *Adv. Funct. Mater.* **2014**, *24*, 2957.
[30] R. Ma, B. Kang, S. Cho, M. Choi, S. Baik, *ACS Nano* **2015**, *9*, 10876.
[31] X. Zhao, F. Chen, Y. Li, H. Lu, N. Zhang, M. Ma, *Nat. Commun.* **2018**, *9*, 3579.
[32] F. Sun, M. Tian, X. Sun, T. Xu, X. Liu, S. Zhu, X. Zhang, L. Qu, *Nano Lett.* **2019**, *19*, 6592.
[33] S. Jiang, H. Zhang, S. Song, Y. Ma, J. Li, G. H. Lee, Q. Han, J. Liu, *ACS Nano* **2015**, *9*, 10252.
[34] K. W. Oh, H. J. Park, S. H. Kim, *J. Appl. Polym. Sci.* **2003**, *88*, 1225.
[35] Y. Ding, W. Xu, W. Wang, H. Fong, Z. Zhu, *ACS Appl. Mater. Interfaces* **2017**, *9*, 30014.
[36] Z. He, J.-H. Byun, G. Zhou, B.-J. Park, T.-H. Kim, S.-B. Lee, J.-W. Yi, M.-K. Um, T.-W. Chou, *Carbon* **2019**, *146*, 701.
[37] Z. Tang, S. Jia, F. Wang, C. Bian, Y. Chen, Y. Wang, B. Li, *ACS Appl. Mater. Interfaces* **2018**, *10*, 6624.
[38] Q. Fan, X. Zhang, Z. Qin, *J. Macromol. Sci., Part B: Phys.* **2012**, *51*, 736.
[39] A. I. Hofmann, I. Östergren, Y. Kim, S. Fauth, M. Craighero, M. H. Yoon, A. Lund, C. Müller, *ACS Appl. Mater. Interfaces* **2020**, *12*, 8713.
[40] A. J. Granero, P. Wagner, K. Wagner, J. M. Razal, G. G. Wallace, M. in het Panhuis, *Adv. Funct. Mater.* **2011**, *21*, 955.
[41] Q. Gao, M. Wang, X. Kang, C. Zhu, M. Ge, *Compos. Commun.* **2020**, *17*, 134.
[42] G. Tian, J. Zhou, Y. Xin, R. Tao, G. Jin, G. Lubineau, *Polymer* **2019**, *177*, 189.
[43] J. Zhou, E. Q. Li, R. Li, X. Xu, I. A. Ventura, A. Moussawi, D. H. Anjum, M. N. Hedhili, D.-M. Smilgies, G. Lubineau, S. T. Thoroddsen, *J. Mater. Chem. C* **2015**, *3*, 2528.
[44] Y. Kim, A. Lund, H. Noh, A. I. Hofmann, M. Craighero, S. Darabi, S. Zokaei, J. I. Park, M.-H. Yoon, C. Müller, *Macromol. Mater. Eng.* **2020**, *305*, 1900749.
[45] M. Wang, Q. Gao, J. Gao, C. Zhu, K. Chen, *J. Mater. Chem. C* **2020**, *8*, 4564.
[46] X. Wang, X. Fu, D. D. L. Chung, *J. Mater. Res.* **1999**, *14*, 790.
[47] J. R. Bautista-Quijano, P. Pötschke, H. Brünig, G. Heinrich, *Polymer* **2016**, *82*, 181.

[48] S. Seyedin, P. Zhang, M. Naebe, S. Qin, J. Chen, X. Wang, J. M. Razal, *Mater. Horiz.* **2019**, *6*, 219.
[49] M. Z. Seyedin, J. M. Razal, P. C. Innis, R. Jalili, G. G. Wallace, *Adv. Funct. Mater.* **2015**, *25*, 94.
[50] S. Seyedin, J. M. Razal, P. C. Innis, G. G. Wallace, *Smart Mater. Struct.* **2016**, *25*, 035015.
[51] A. J. Granero, J. M. Razal, G. G. Wallace, M. in het Panhuis, in *IEEE 2010 Int. Conf. Nanoscience and Nanotechnology (ICONN)*, IEEE, Piscataway **2010**, p. 80.
[52] X. Wang, Y. Qiu, W. Cao, P. Hu, *Chem. Mater.* **2015**, *27*, 6969.
[53] H. Wang, Z. Liu, J. Ding, X. Lepró, S. Fang, N. Jiang, N. Yuan, R. Wang, Q. Yin, W. Lv, Z. Liu, M. Zhang, R. Ovalle-Robles, K. Inoue, S. Yin, R. H. Baughman, *Adv. Mater.* **2016**, *28*, 4998.
[54] J. Eom, R. Jaisutti, H. Lee, W. Lee, J. S. Heo, J. Y. Lee, S. K. Park, Y. H. Kim, *ACS Appl. Mater. Interfaces* **2017**, *9*, 10190.
[55] J. P. Wang, P. Xue, X. M. Tao, *Mater. Sci. Eng. A* **2011**, *528*, 2863.
[56] S. E. Root, S. Savagatrup, A. D. Printz, D. Rodriquez, D. J. Lipomi, *Chem. Rev.* **2017**, *117*, 6467.
[57] B. Roth, S. Savagatrup, N. V. de los Santos, O. Hagemann, J. E. Carlé, M. Helgesen, F. Livi, E. Bundgaard, R. R. Søndergaard, F. C. Krebs, D. J. Lipomi, *Chem. Mater.* **2016**, *28*, 2363.
[58] J. Hynynen, E. Järsvall, R. Kroon, Y. Zhang, S. Barlow, S. R. Marder, M. Kemerink, A. Lund, C. Müller, *ACS Macro Lett.* **2019**, *8*, 70.
[59] R. Xie, R. H. Colby, E. D. Gomez, *Adv. Electron. Mater.* **2018**, *4*, 1700356.
[60] C. Bounioux, P. Díaz-Chao, M. Campoy-Quiles, M. S. Martín-González, A. R. Goñi, R. Yerushalmi-Rozen, C. Müller, *Energy Environ. Sci.* **2013**, *6*, 918.
[61] R. Kroon, A. I. Hofmann, L. Yu, A. Lund, C. Müller, *Chem. Mater.* **2019**, *31*, 2770.
[62] S. Zokaei, R. Kroon, J. Gladisch, B. D. Paulsen, W. Sohn, A. I. Hofmann, G. Persson, A. Stamm, P.-O. Syrén, E. Olsson, J. Rivnay, E. Stavrinidou, A. Lund, C. Müller, *Adv. Sci.* **2021**, *8*, 2002778.
[63] C. B. Nielsen, A. Giovannitti, D.-T. Sbircea, E. Bandiello, M. R. Niazi, D. A. Hanifi, M. Sessolo, A. Amassian, G. G. Malliaras, J. Rivnay, I. McCulloch, *J. Am. Chem. Soc.* **2016**, *138*, 10252.
[64] A. Giovannitti, C. B. Nielsen, D.-T. Sbircea, S. Inal, M. Donahue, M. R. Niazi, D. A. Hanifi, A. Amassian, G. G. Malliaras, J. Rivnay, I. McCulloch, *Nat. Commun.* **2016**, *7*, 13066.
[65] A. Savva, R. Hallani, C. Cendra, J. Surgailis, T. C. Hidalgo, S. Wustoni, R. Sheelamanthula, X. Chen, M. Kirkus, A. Giovannitti, A. Salleo, I. McCulloch, S. Inal, *Adv. Funct. Mater.* **2020**, *30*, 1907657.
[66] A. Giovannitti, D.-T. Sbircea, S. Inal, C. B. Nielsen, E. Bandiello, D. A. Hanifi, M. Sessolo, G. G. Malliaras, I. McCulloch, J. Rivnay, *Proc. Natl. Acad. Sci. USA* **2016**, *113*, 12017.
[67] J. Brebels, J. V. Manca, L. Lutsen, D. Vanderzande, W. Maes, *J. Mater. Chem. A* **2017**, *5*, 24037.
[68] D. Kiefer, A. Giovannitti, H. Sun, T. Biskup, A. Hofmann, M. Koopmans, C. Cendra, S. Weber, L. J. Anton Koster, E. Olsson, J. Rivnay, S. Fabiano, I. McCulloch, C. Müller, *ACS Energy Lett.* **2018**, *3*, 278.
[69] J. Liu, L. Qiu, R. Alessandri, X. Qiu, G. Portale, J. Dong, W. Talsma, G. Ye, A. A. Sengrian, P. C. T. Souza, M. A. Loi, R. C. Chiechi, S. J. Marrink, J. C. Hummelen, L. J. A. Koster, *Adv. Mater.* **2018**, *30*, 1704630.
[70] B. Meng, J. Liu, L. Wang, *Polym. Chem.* **2020**, *11*, 1261.
[71] D. Ohayon, G. Nikiforidis, A. Savva, A. Giugni, S. Wustoni, T. Palanisamy, X. Chen, I. P. Maria, E. Di Fabrizio, P. M. F. J. Costa, I. McCulloch, S. Inal, *Nat. Mater.* **2020**, *19*, 456.
[72] C. K. Song, B. J. Eckstein, T. L. D. Tam, L. Trahey, T. J. Marks, *ACS Appl. Mater. Interfaces* **2014**, *6*, 19347.
[73] D. Moia, A. Giovannitti, A. A. Szumska, I. P. Maria, E. Rezasoltani, M. Sachs, M. Schnurr, P. R. F. Barnes, I. McCulloch, J. Nelson, *Energy Environ. Sci.* **2019**, *12*, 1349.
[74] A. V. Volkov, H. Sun, R. Kroon, T.-P. Ruoko, C. Che, J. Edberg, C. Müller, S. Fabiano, X. Crispin, *ACS Appl. Energy Mater.* **2019**, *2*, 5350.
[75] R. Kroon, D. Kiefer, D. Stegerer, L. Yu, M. Sommer, C. Müller, *Adv. Mater.* **2017**, *29*, 1700930.
[76] J. Li, C. W. Rochester, I. E. Jacobs, E. W. Aasen, S. Friedrich, P. Stroeve, A. J. Moulé, *Org. Electron.* **2016**, *33*, 23.
[77] A. I. Hofmann, R. Kroon, L. Yu, C. Müller, *J. Mater. Chem. C* **2018**, *6*, 6905.
[78] R. Kroon, J. D. Ryan, D. Kiefer, L. Yu, J. Hynynen, E. Olsson, C. Müller, *Adv. Funct. Mater.* **2017**, *27*, 1704183.
[79] J. Moulton, P. Smith, *Synth. Met.* **1991**, *40*, 13.
[80] J. Moulton, P. Smith, *Polymer* **1992**, *33*, 2340.